



Experimental investigation of performance and soot emissions of oxygenated fuel blends in a small aero engine

Alexander Rabl¹ · Christopher Mull¹ · Martin Härtl² · Christian Helcig¹ · Volker Gümmer¹

Received: 22 February 2023 / Revised: 10 October 2023 / Accepted: 23 October 2023 / Published online: 7 November 2023
© The Author(s) 2023

Abstract

Recent studies show that mixing jet fuel with oxygenated fuels has an impact on exhaust gas soot formation. Soot particles are an environmental hazard with an impact on air quality around airports, and possibly influencing ice crystal nucleation, leading to contrail and ice cloud (cirrus) formation. These ice clouds significantly warm up the atmosphere by reflecting heat radiation back to Earth and, at the same time, being transparent to incoming sunlight. Many investigations concentrate on reducing aviation's CO₂ footprint, but only a few account for reducing soot emissions in aero engines. This study examines the potential of blending Jet A-1 with oxygenated fuels to decrease soot particle formation in aero engines. For this, blends with 5 vol% and 20 vol% of ethanol, and 5 vol% of a polyoxymethylene dimethyl ether 3–5 mix (OME3-5 mix) are investigated in an Allison 250-C20B turboshaft engine with the help of a condensation particle counter (CPC). The results show tendencies in soot particle reduction, which, in most cases, is larger than the volumetric percentage of the oxygenated fuel within the blend.

Keywords Jet A-1 blends · Oxygenated fuels · SAF · Aero engines

Abbreviations

ASG	Analytik-Service Gesellschaft
ASTM	American Society for Testing and Materials
CDAS	Continuous data acquisition system
CO ₂	Carbon dioxide
CPC	Condensation particle counter
DSU	Direct sampling unit
E20	Jet A-1, blended with 20 vol% bio ethanol
E5	Jet A-1, blended with 5 vol% bio ethanol
ET	Evaporation tube
GI	Ground idle
HL	High load
Jet	Neat Jet A-1
LHV	Lower heating value [MJ/kg]

LL	Low load
ML	Medium load
O5	Jet A-1, blended with 5 vol% OME3-5 mix
OESI	Oxygen-Extended Sooting Index
OME _(n)	Polyoxymethylene dimethyl ether (of the chain length n)
PCF	Pre-classifier cyclone
PCRF	Particle concentration reduction factor
PND	Diluter
SPCS	Solid particle counting system
TO/GA	Take-off and go-around
VPR	Volatile particle remover

List of symbols

D_f	Total dilution factor
D_{50}	Counting efficiency
m%	Mass percent
n	Number of particles
N_{total}	Absolute particle concentration
Q_{dil}	Dilution flow [l/min]
σ	Standard deviation
$\bar{\sigma}$	Mean standard deviation
vol%	Volume percent

Alexander Rabl and Christopher Mull have contributed equally to this work.

✉ Alexander Rabl
alexander.rabl@tum.de

¹ Chair of Turbomachinery and Flight Propulsion, Technical University of Munich, Boltzmannstr. 15, 85748 Garching, Germany

² Chair of Sustainable Mobile Drivetrains, Technical University of Munich, Schragenhofstr. 31, 80992 Munich, Germany

1 Introduction

Due to the limited availability of electric or hydrogen aircraft and their short mission range capability, drop-in fuels are the means of choice to reduce aviation's carbon footprint in the short term. Besides the beneficial environmental effect of carbon-neutral drop-in fuels regarding their carbon footprint, they also offer the possibility of significantly reducing non-CO₂ effects like contrail-induced cirrus clouds [1]. Many studies have already shown the substantial adverse environmental impact of contrails and contrail-induced cirrus cloud coverage caused by aviation [2–6] and, therefore, the need to minimize these so-called non-CO₂ emissions. These contrails are formed primarily because of soot particle emission initiating ice crystal nucleation under certain atmospheric conditions. Water within the supersaturated air of the exhaust jet first condenses, accumulates, and then freezes on the soot particle surfaces, leading to bigger ice crystals forming the visible contrail cirrus [5, 7, 8]. These contrails and contrail-induced cirrus cloud coverage heat Earth's atmosphere on one hand by reflecting heat radiation coming from the ground back to Earth. On the other hand, these clouds are transparent to incoming sun rays that heat the Earth further. Mitigation of this effect is possible by reducing soot emissions from jet engine combustion. Soot particle emission is primarily caused by incomplete combustion, e.g., in fuel-rich flames or cold combustion temperatures within the engine's combustion chamber [9–11]. When using carbon-neutral drop-in fuels, the reduction in soot emissions is accomplished mainly by the lack of aromatic content, leading to better combustion. Newly published studies on laboratory flames show that soot emission reduction can also be achieved by blending jet fuel with oxygen-containing fuel components, known as oxygenated fuels [12]. These investigations show a substantial decrease in the OESI—the Oxygen-Extended Sooting Index—even at very low blend ratios from 5 to 20 vol% of ethanol and polyoxymethylene dimethyl ethers 1 and

3 (OME1, OME3) to Jet A-2. As a result, a reduction of the OESI down to -40% and more was achieved. Furthermore, laboratory experiments with OME1 flames demonstrated entirely soot-free combustion [13]. Experimental investigations with heavy-duty internal combustion diesel engines indicate that this trend also holds for higher OME molecules such as OME 3–6, although not being as strong [14]. So far, OME has been primarily considered a regenerative alternative diesel fuel. However, its physical and chemical properties are very close to jet fuel (see Table 1). It is also well known for its soot-reducing effect during combustion because of its lack of direct carbon-carbon bonds within its molecular structure. These facts make it a very interesting candidate as a blend-in component for jet fuel. Meanwhile, ethanol is more established as a gas turbine fuel or blend component and is known for its positive effect on general emission characteristics in aero engines [15, 23–26]. Both fuels show good prospects for synergy effects with the automotive sector on mass-scale production, fair prices, and availability. Additionally, ethanol is already produced worldwide in vast amounts as a regenerative drop-in fuel for gasoline. That said, speaking of ethanol and OME as drop-in fuel for jet fuel might not be correct since such a blend could only meet ASTM jet fuel requirements at very low volumetric blend ratios, primarily because of the stringent heating value demand of ASTM D1655. Therefore, ethanol jet fuel blends with no more than 2.9 vol% or blends with no more than 2.7 vol% OME3-5 mix are feasible to meet these standards. When raising the portion of these fuels further, additional jet fuel specification permissions must be made. Consequently, speaking of ethanol and OME as blend-in fuels seems more reasonable. This paper examines the effect of 5–20 vol% of ethanol and OME3-5 mix on soot emissions with real-life scale aero engine tests.

The energy content for Jet A-1 and Jet B are the lowest allowed Heating values regarding ASTM D 1655 [21]. OME properties are partially given by the laboratory analysis from the fuel distributor ASG (Analytik-Service Gesellschaft).

Table 1 Physical and chemical properties of Jet A-1, OME3-5 mix, ethanol, and Jet B [15–22]

Properties	Jet A-1	OME3-5 Mix	Ethanol	Jet B
O/C Ratio	–	0.8	0.5	–
Boiling range [°C]	180–260	156–242	78	50–260
Flash point [°C]	38	54–115	12.7	–20
Freezing point [°C]	–47 (–40 Jet A-2)	–43 to (+18)	–130.5	–60
Density @15 °C [kg/m ³]	775–840	1068	794	810
Kin. Visc. @ –20 °C [Cst]	8	1.19(@40°C)	3.44	–
Energy [MJ/kg]	42.8	19.11	26.8	42.8

Table 2 Allison 250-C20B technical data

Properties	Unit	Value
Weight	kg	72
Length	mm	986
Width	mm	483
Height	mm	597
Max. power	kW	313
Max continuous	kW	298
Power/weight ratio (max.)	kW/kg	4.35:1
Max. air intake	kg/s	1.56
Max. pressure ratio	–	7.1
Power shaft (100%)	1/min	6016
Gas generator rpm (100%)	1/min	50,970
Power turbine rpm (100%)	1/min	33,290

2 The Allison 250-C20B test rig

For these tests, an Allison 250-C20B turboshaft engine, mainly operated by helicopters and fixed-wing turboprop aircraft is used. Aero engine soot emission in high-altitude operations like aircraft cruise flight can have a major climate impact due to induced contrail formation if certain atmospheric conditions apply [4]. Also, local soot emission during aircraft taxi, landing, and take-off can have a negative impact on the environment and human health [27]. In general, the thermodynamic principle of the aero engine gas turbine can be adapted to all currently used aero engine types. Further investigation of its soot emission is therefore necessary. For technical data on the Allison engine used, refer to Table 2. The absolute particle matter emissions of different engine types may differ because of different pressure ratios and combustion chambers. Although current knowledge about the exact influence of elevated pressures on soot formation and morphology—as well as its impact on possible induced contrail formation—is scarce, general sooting tendency trends are preserved [28]. Therefore, the relative soot reduction because of different fuel blends remains representative. Furthermore, the use of a smaller turboshaft aero engine allows for better test rig integration since its power output is directly measurable as shaft horsepower. This happens with the help of an eddy current brake. The test rig has sensors to monitor the different engine stage's pressure, temperatures, and rotational speed. The fuel flow is measured by a dynamic balance that indicates the gravimetric fuel consumption per second. The whole thermodynamic cycle of the engine can be calculated using temperature and pressure sensor data. The particle emission probe is mounted at one of the two exhaust ducts. It consists of a metal tube reaching the middle of the exhaust duct diameter. The metal tube tip is cut-off at a 45-degree angle, and its opening points in a streamwise direction to avoid blockage due to big particles

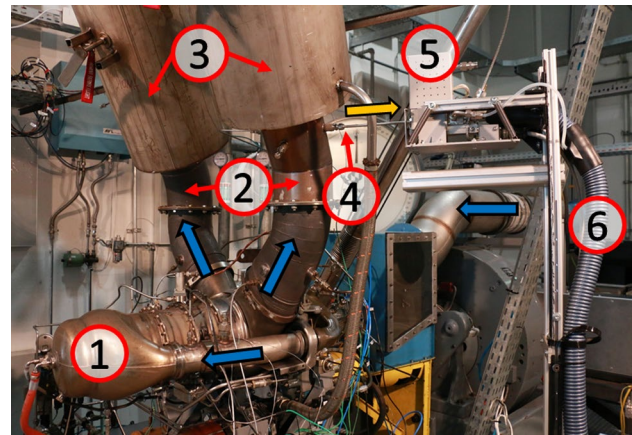


Fig. 1 Allison 250-C20B test rig with combustion chamber (1), exhaust pipes (2), exhaust chimneys (3), sample probe (4), direct sampling unit (5), and heated sample gas line (6). The engine gas path is marked with blue arrows and the sampling path with an orange arrow

being streamed directly into the probe. Samples are then led through the probe to the DSU, the direct sampling unit, which is the input sampler of the particle measurement system. A picture of the Allison 250 test rig with the mounted DSU (5) is depicted in Fig. 1. Furthermore, the combustion chamber (1), the exhaust pipes (2), the exhaust chimneys (3), the particle sampling probe (4), and the particle sample gas line (6) are identified by numbers. Additionally, the gas path is illustrated by blue arrows and the particle sampling path by an orange arrow.

3 The MEXA-2100SPCS particle counting system

The particle measurement is conducted with a MEXA-2100SPCS system manufactured by Horiba. It is based on the newest UN/ECE Regulation No. 83 (Rev. 4) for particle emission measuring and features a CPC100 unit as a condensation particle counter (CPC) made by TSI. After sampling and pre-heating using the DSU, the sample gas reaches the pre-classifier cyclone (PCF) via a heated hosepipe. It removes particles larger than 2.5 μm . The smaller particles are then guided to the volatile particle remover (VPR). The VPR consists of a primary diluter (PND1), an evaporation tube (ET), and a secondary diluter (PND2). PND1 heats the sample to more than 150 $^{\circ}\text{C}$ to prevent the formation of volatile particles and dilutes the sample further. After that, the diluted gas sample reaches the heated evaporation tube to vaporize all already formed particles. This happens at 300 $^{\circ}\text{C}$ to 400 $^{\circ}\text{C}$ to prohibit the production of new volatile particles via re-condensation. After that, the gas concentration is further reduced by PND2, which also cools the temperature down by diluting it with air at room temperature. By cooling

via dilution, the loss of particles due to thermal migration is also reduced. The solid particles that pass through the VPR are then led into the CPC100. The sample gas is saturated with butanol vapor within the condensation particle counter at first. After that, it is led into a cooled condenser, where the butanol vapor reaches a supersaturated state and starts to condense on the solid particle surfaces. With ongoing nucleation, the particles grow into larger particles that are big enough to be detected by the optical laser counting unit. A critical orifice at the end of the tube system keeps the sample gas flow at 1.0 l/min. Therefore, the dilution flow Q_{dil} never reaches or exceeds 1.0 l/min. The total dilution factor D_f is then calculated by

$$D_f = \frac{1 \frac{l}{min}}{1 \frac{l}{min} - Q_{dil}}. \quad (1)$$

Since the CPC unit only counts the total number of particles detected (n), the absolute particle concentration N_{total} is given by

$$N_{total} = n \cdot D_f. \quad (2)$$

These calculated values are given as readouts in the Horiba software for the MEXA-2100SPCS. The particle concentration reduction factor (PCRF), which is typically used to quantify particle losses in the system, is not used during this test series since no exact calibration data for the PCRF

for this test setup are available yet. However, because only the relative particle reduction between the different blends is of importance, statements based on the particle concentration calculated via the total dilution factor are still valid. The schematic setup of the whole system is shown in Fig. 2. The counting efficiency of the CPC is $D_{50} = 10\text{nm}$, which means it can still detect 50% of all particles with a diameter of 10 nm. The detailed counting efficiency curve is given in [29]. But, for this study, no correction regarding the counting efficiency was done. The literature shows that for the Allison engine, no particle emissions are expected below 10 nm in diameter [30], and therefore, the lower detection limit of the system is considered sufficient.

4 Experimental procedure

Before the conduction of the actual tests, some pre-examinations are made to verify the compatibility of the fuel system with the new blends. For this, the prevailing seals of the fuel lines within the system are exposed to the different blends for at least 72 h. The results show that the maximum amount of OME3-5 mix blended with jet fuel should not exceed 5 vol% when using the existing seals. Otherwise, swelling would be an issue. For ethanol, no such concerns are raised after these tests. Therefore, the blend ratios with Jet A-1 (Jet) for the tests are specified as 5 vol% (4.99 m%) and 20 vol% (19.96 m%) of ethanol (E5, E20) and 5 vol%

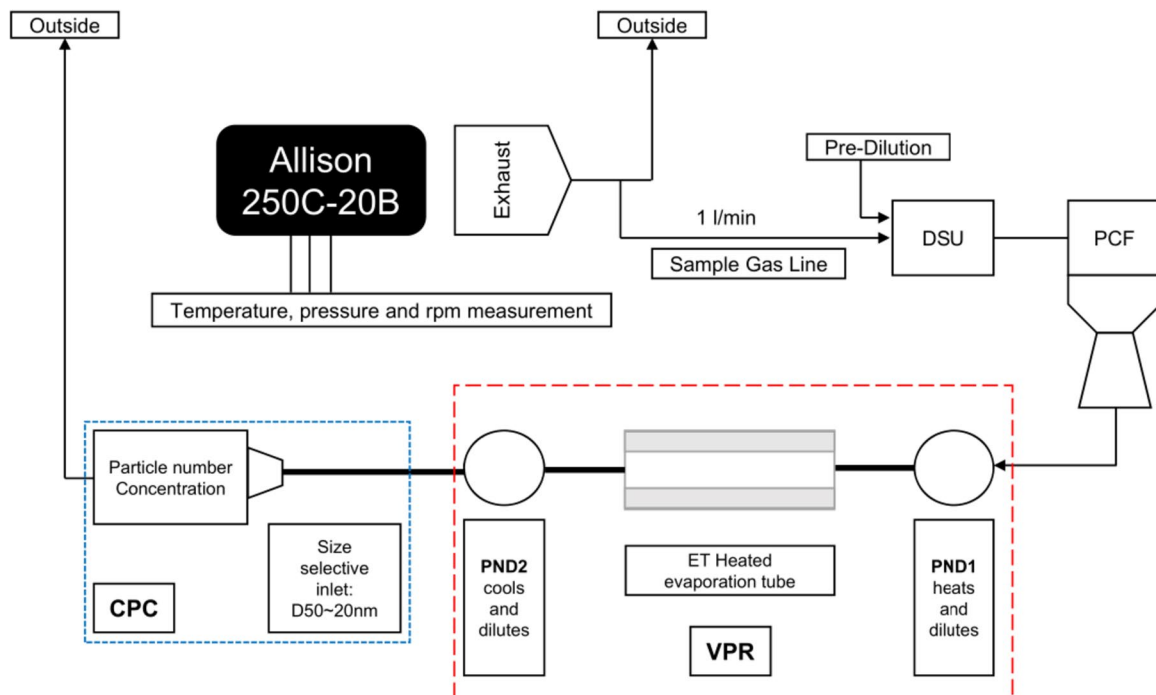


Fig. 2 Schematic engine particle emission measuring system

Table 3 Lower fuel heating value of the utilized Jet A-1 (Jet) and calculated values for E5, E20, and 5 vol% OME3-5 mix (O5)

Blend	Jet	E5	E20	O5
Energy [MJ/kg]	43.271	42.45	39.98	41.68

(6.59 m%) of OME3-5 mix (O5). These blend ratios also suit the investigated blends of the previous study by Tan et al. [12]. Table 3 shows the calculated lower fuel heating values of the blends. Taking heating value and sealing compatibility into account, two major compliance points regarding Jet fuel standards are addressed. It should be noted that further fuel critical properties of these blends like oxygen content or other chemical/physical characteristics would need major revision of current ASTM Jet fuel standards to allow such blends in commercial operation. The E5 and O5 blends are each tested three times. The E20 blend is tested two times. Each test run starts with a period of purging the fuel lines during engine idle until only the new fuel blend persists in the fuel lines. After that, the test envelope is carried out two times per test run. The test envelope consists of the ground idle (GI), a low load condition (LL) which equals 100 Nm of torque, a medium load condition (ML) for cruise conditions (200 Nm torque), and a high load condition (HL) with 300 Nm torque load. Those load conditions were chosen since they represent the whole operating range of the engine. GI represents the lowest possible load condition of the engine. HL represents a take-off load condition, which is one of the highest possible engine load conditions. LL and ML are intermediate load conditions to allow for better detection of possible trends over the whole operating range. Only the second envelope cycle results are taken and further processed to ensure the engine is in a warm operating condition. For the same reason, the ground idle state is only captured at the end of each envelope cycle. For Jet A-1, the test envelope is performed eight times to build a reference baseline.

4.1 Conduction of measurement

Before starting a measurement series, all measurement equipment is pre-heated for at least 30 minutes, and the particle sampling system lines are purged. This ensures that the measurement systems are running stable and that no particles from earlier test runs influence the results. After stabilizing and purging, for each test envelope state, a particle counter measurement of a minimum of 30 seconds is performed. The sample rate of the particle measurement is set to 1 Hz so that, in total, at least 30 samples at each load setting are taken. The dilution factor of the DSU in combination with the PND1 is adjusted to 500, and the dilution of the PND2 is fixed at 15. This results in a total dilution factor of $D_f = 7500$. With this total dilution factor, the raw particle

Table 4 Error margins during the measurement. The data are given for ground idle (GI), low load (LL), medium load (ML), and high load (HL). The values σ and $\bar{\sigma}$ are given in particles per cubic centimeter [$\#/cm^3$]

Component	$\sigma \cdot 10^6$	$\bar{\sigma} \cdot 10^6$
GI Jet	6.95	1.92
GI O5	3.12	1.31
GI E5	4.70	1.16
GI E20	1.32	1.16
LL Jet	9.16	1.46
LL O5	4.04	1.59
LL E5	5.69	1.91
LL E20	2.32	1.04
ML Jet	8.30	1.88
ML O5	5.21	1.42
ML E5	5.71	1.74
ML E20	1.89	1.26
HL Jet	7.59	1.32
HL O5	3.63	1.64
HL E5	5.05	1.25
HL E20	1.80	1.27

count is always in the range of what the CPC can handle, and no additional correction factors must be considered. After each different fuel blend, sample lines of the particle sampling system are purged again. The Continuous Data Acquisition System (CDAS) of the Allison test rig samples at 10 Hz. The data sets of the Allison are matched with the Horiba SPCS data via manual matching with the help of a triggered series set at the different measurement points. Checking and processing the data and creating the graphs are done using MatLab.

4.2 Reproducibility

All measured particle concentration values during one sample are averaged. The related standard deviations are given in Table 4. The standard deviation of each sample set for every load state is large compared to the mean values. This is due to the fact that the deviation in particle concentration during sampling is most likely related to unsteadiness within the engine and its combustion and not caused by random measurement system errors. The standard deviations of the different load settings of each blend are averaged over the three (O5, E5) and two (E20) runs, respectively, conducted to gather better confidence in the results. This averaged standard deviation, given in Table 4 as $\bar{\sigma}$, illustrates how much noise is normally expected within the sample signal.

If the different test runs for the same fuel blend are conducted on different days with other ambient conditions, this value may stay more or less within the same range, but the overall average point of the particle concentration for the sample may differ to a greater extent. If all values of every test run for each load setting are considered as one data set, the obtained standard deviation is then defined as σ . This

value can be interpreted as the reproducibility of a test run, also given in Table 4. Because, as mentioned before, environmental and engine conditions slightly differ for every test run, the standard deviation σ may be considered as large. Still, the resulting mean particle concentration is taken into account as a good indication of the mean expected emissions gathered over long-time operation in different conditions.

5 Results and discussion

The following graphs (Figs. 3, 4, 5, 6) show the results of the mean particle concentration measured in particles per cubic centimeter [$1/\text{cm}^3$] on the y-axis. Each bar represents a different fuel blend, marked on the x-axis. The number on the bottom of each bar—apart from Jet A-1—is the mean particle concentration reduction percentage compared to Jet A-1. The corresponding standard deviation for each chart and bar is given in Table 4, as mentioned above. Also, the reproducibility σ is indicated as hash marks in the figures. Figure 3 shows the results in the ground idle state. The O5 blend shows a percentage particle reduction of 17%, the E5 blend 9%, and the E20 blend 32%. Even though the OME blend only contains 5 vol% OME3-5 mix, the percentage reduction of particle concentration (-17%) is more than three times higher than its volumetric content, in contrast to E5 and E20, which generates a percentage

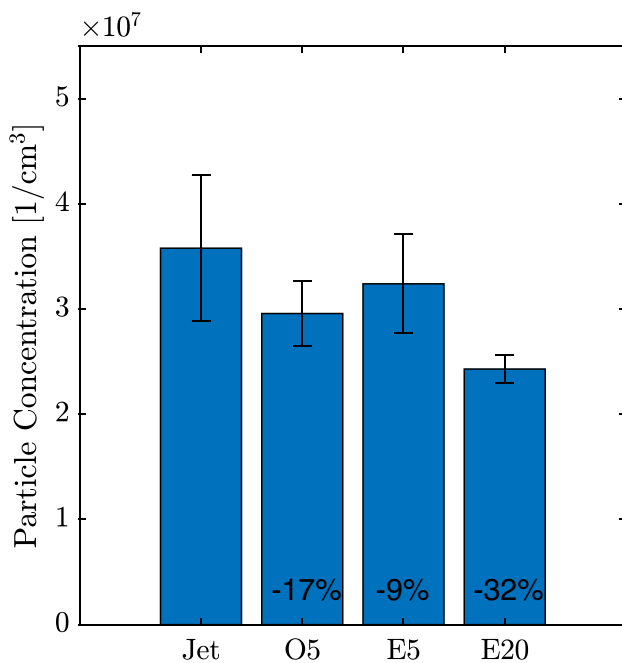


Fig. 3 Particle concentration for Jet A-1, E5, E20, and 5 vol% OME3-5 mix (O5) at ground idle (GI). The percentage particle concentration reduction compared to Jet A-1 is indicated at each bar. The whiskers represent the value σ from Table 4

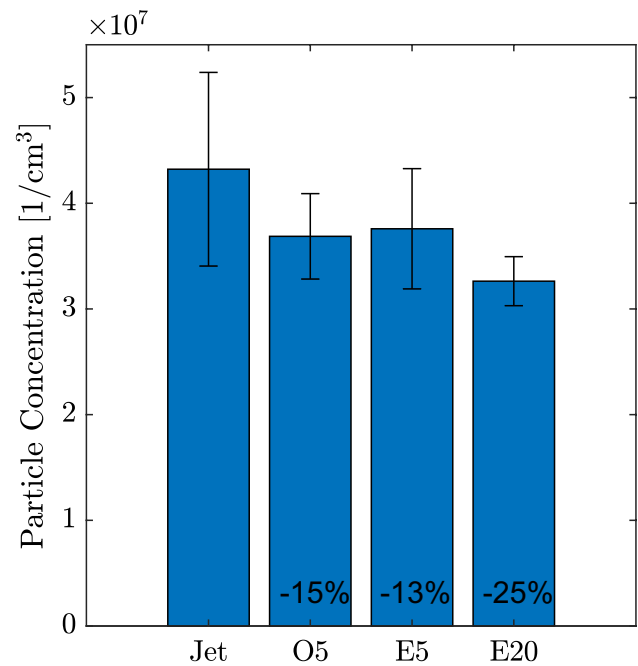


Fig. 4 Particle concentration for Jet A-1, E5, E20, and 5 vol% OME3-5 mix (O5) at low load (LL). The percentage particle concentration reduction compared to Jet A-1 is indicated at each bar. The whiskers represent the value σ from Table 4

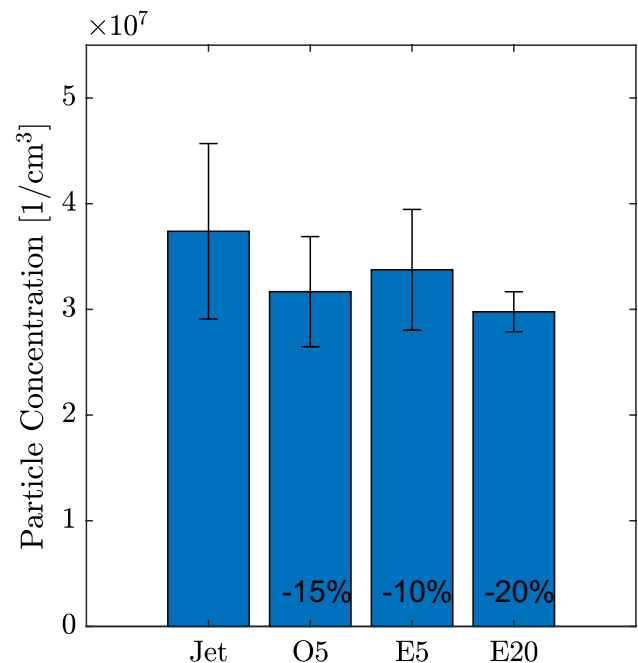


Fig. 5 Particle concentration for Jet A-1, E5, E20, and 5 vol% OME3-5 mix (O5) at medium load (ML). The percentage particle concentration reduction compared to Jet A-1 is indicated at each bar. The whiskers represent the value σ from Table 4

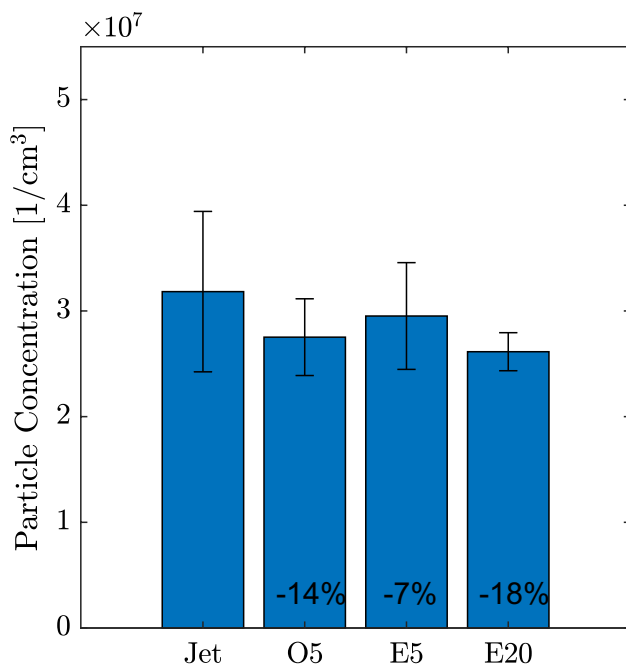


Fig. 6 Particle concentration for Jet A-1, E5, E20, and 5 vol% OME3-5 mix (O5) at high load (HL). The percentage particle concentration reduction compared to Jet A-1 is indicated at each bar. The whiskers represent the value σ from Table 4

particle concentration reduction not even twice as much as the volumetric blend-in ratio. That being said, the E20 blend still shows with 32% reduction, the highest absolute decrease in particle concentration of the whole test series. The same trend can be seen in Fig. 4, which shows the mean values for a low load state (ca. 100 Nm torque). In this state, E5 performs slightly better than at ground idle. The reduction effect of E20 is lower, on the other hand. The O5 blend performs comparably to ground idle. The same happens for the medium load state (Fig. 5) apart from E20, performing approximately 5% worse in terms of percentage particle concentration reduction within the exhaust gas. Figure 6 shows the maximum load condition, which comes closest to the TO/GA (take-off and go-around) condition. For this case, the O5 blend shows a reduction of 14%, roughly three times the amount of the volumetric blend ratio itself. The E5 blend shows a reduction of 7% for this case, which is in the same range as for the other load cases. The percentage reduction for the E20 blend, on the other hand, is 18%, which is even lower than the blending ratio of 20 vol%. The O5 blend shows the most favorable behavior since its particle concentration reduction effect is steady over the whole test envelope. Additionally, the O5 blend shows a reduction in the particle concentration of roughly three times as much as the blend ratio (5 vol%) for every load setting. In contrast, E20 shows strong reduction effects primarily in the lower load states and ground idle. E5 performs better

than E20 overall relative to its percentage volumetric blend-in content. The results indicate that higher oxygen content of the fuel leads to lower particle emissions. This happens as expected because, in the case of fuel-bounded oxygen, less oxygen coming from the oxidizer (air) must diffuse into the flame required for complete combustion. It, therefore, affects the flame length and consequently the smoke point [12]. Also, due to the lack of intermolecular carbon-carbon bonds, the OME3-5 mix is less likely to form soot precursors such as acetylene and polycyclic aromatic hydrocarbons during combustion [31]. Ethanol still contains a carbon-carbon bond that can lead to ethene, which may lead to or interact with jet fuel for soot formation [32]. Another reason for the lower soot production, when blending oxygenates, is the increased formation of soot-suppressing OH^* and CH_3O^* radicals during alcohol or OME combustion [33]. Considering the volumetric blend ratios, the O5 blend exhibits more favorable behavior than the E5 blend. When normalizing the results to the calculated percentage oxygen content of the fuel blends (O5 = 3.18 O_2 -m%, E5 = 1.74 O_2 -m%, and E20 = 6.94 O_2 -m%), the O5 blend still demonstrates a greater percentage reduction in soot for GI and HL. However, for LL and ML, using the E5 blend results in a larger reduction normalized to the oxygen content. Looking at the Allison engine, the more relevant load settings are GI and HL, since GI is mainly on the ground where soot can impact human health and HL is close to the TO/GA condition, where the engine operates for the longest time period. Therefore, the O5 blend is still considered slightly preferable compared to the E5 blend when solely taking soot particle reduction into account. If aiming for the highest soot particle reduction while adding as little fuel-bound oxygen as possible, the E5 blend is preferable. However, considering the reproducibility of the conducted experiments, the result provides only a tendency, which requires further validation.

5.1 Processed data

While the results shown above indicate the volumetric particle concentration in the exhaust gas, they do not answer how “clean” the combustion in general is. This is because the absolute volume flow of the exhaust gas and the corresponding fuel flow differ significantly at different load states of the engine. Therefore, the particle concentration is standardized with its fuel flow of each load stage in the first step. The different fuel consumption rates for each load setting and every blend are shown in Fig. 7. In this chart, the fuel flow data from eight Jet A-1 runs, three O5 and E5 runs, and two E20 runs are averaged. The gravimetric fuel flow in [g/s] is indicated on the y-axis. On the x-axis, the different load settings are marked. As expected, the fuel flow for the lowest load setting (GI) is the lowest and increases steadily for higher load settings. But with changing fuel heating values

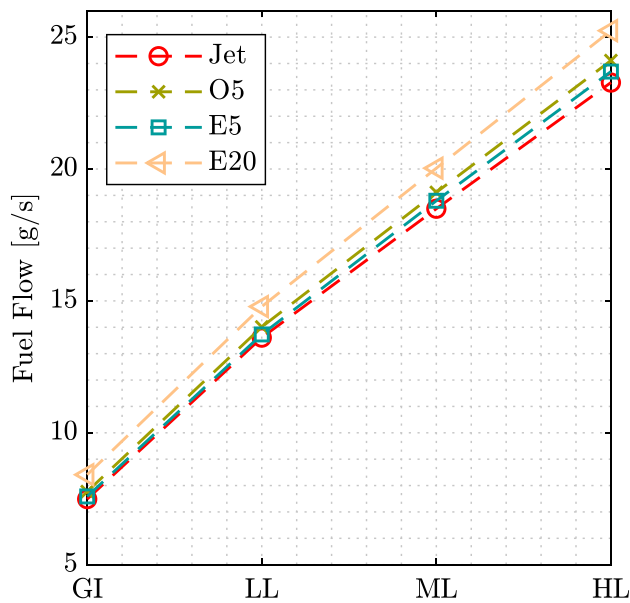


Fig. 7 Measured fuel flow at investigated load settings for Jet A-1, E5, E20, and 5 vol% OME3-5 mix (O5)

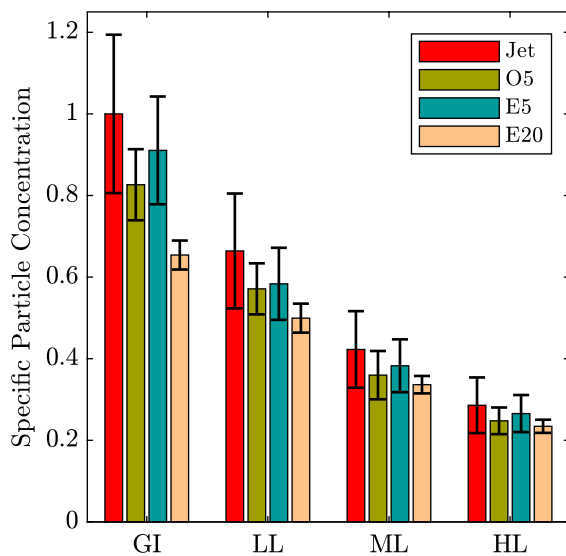


Fig. 8 Specific particle concentration for Jet A-1, E5, E20, and 5 vol% OME3-5 mix (O5). The values of each bar are sorted by load setting and normalized to the result for Jet A-1 at GI. The whiskers represent the normalized values σ from Table 4

of the blends—as shown in Table 3—the necessary fuel flow for the same heat input during combustion also differs for every blend. Comparing the different blends regarding fuel consumption indicates that neat Jet A-1 has the lowest fuel consumption. The use of E5 only leads to slightly higher fuel demand. For the O5 and E20 blends, the consumption rates rise more distinctively. Therefore, the fuel-normalized

data must be normalized again with the specific gravimetric energy content of the fuel blends—the lower heating value (LHV)—to make particle emission data comparable between the different blends. These results are shown in Fig. 8. Herein, the specific particle concentration is defined on the y-axis. It gives the number of particles per cubic centimeter ($1/\text{cm}^3$) normalized by the gravimetric fuel flow (kg/s) and the lower heating value (MJ/kg). After that, the resulting particle concentration is normalized by the highest occurring particle concentration measured. Therefore, this figure shows the particle concentration per energy input normalized to the particle concentration of the GI load setting when using neat Jet A-1. The same normalization is also applied to the reproducibility σ and is shown as whiskers in Fig. 8. With this representation, the influence of different amounts of fuel and varying lower heating values is considered. It can be seen that the specific amount of particles produced at GI is the worst and gets better for higher loads. Still, the qualitative results regarding the percentage particle reduction between the different blends compared to Jet A-1 stay the same. Quantitatively speaking, the reduction is still in the same order of magnitude and differs not much from the percentage reductions indicated in Figs. 3, 4, 5, 6. This is because the increase in gravimetric fuel consumption when using the blends is approximately inversely proportional to the decrease in the LHV of the blends. What changes significantly is the relation between the different load settings, indicating that low load conditions, like ground idle, cause bad combustion quality with high specific particle emissions, even though the absolute particle concentration values of the exhaust gas might be lower compared to other load scenarios.

6 Conclusion and outlook

The present work examines the impact of blending small amounts of oxygenated fuels to regular Jet A-1 on the particle concentration in the exhaust fumes of a turboshaft engine (Allison 250-C20B). The tested blending fuels included an OME3-5 mix and ethanol. In general, for all investigated blends and load settings, a percentage reduction in particle concentration can be observed, as previously reported for single flame combustion experiments. Concerning the volumetric blending ratio, the most promising blending fuel was the OME3-5 mix. When focusing on the percentage of oxygen mass content, it remains inconclusive whether the E5 or the O5 blend performs better. Blending OME3-5 or ethanol with regular Jet A-1 in small amounts is a quick measure to reduce the amount of soot in jet engine exhausts and, by that, possibly reduce ground-based environmental impact and the generation of contrail-induced emissions. For further consolidation and a deeper understanding of the findings

of the present work, the following steps are recommended: first, the errors occurring in the particle measurement have to be reduced. Also, further tests with the blends should be conducted. In this context, the gaseous emissions are also to be analyzed. In addition, other blend ratios with the OME3-5 mix could be carried out, especially with lower blending ratios, like 2.9 vol%. By blending such a low amount with regular Jet A-1, the properties of the blend would still fit or at least be close to the limits of the ASTM D1655 Norm for jet fuel.

Funding Open Access funding enabled and organized by Projekt DEAL. The authors gratefully thank Munich Aerospace e.V.—Bavarian Research Alliance, who supported and funded this project.

Declarations

Conflict of interest The authors have no competing interests to declare that are relevant to the content of this article.

Open Access This article is licensed under a Creative Commons Attribution 4.0 International License, which permits use, sharing, adaptation, distribution and reproduction in any medium or format, as long as you give appropriate credit to the original author(s) and the source, provide a link to the Creative Commons licence, and indicate if changes were made. The images or other third party material in this article are included in the article's Creative Commons licence, unless indicated otherwise in a credit line to the material. If material is not included in the article's Creative Commons licence and your intended use is not permitted by statutory regulation or exceeds the permitted use, you will need to obtain permission directly from the copyright holder. To view a copy of this licence, visit <http://creativecommons.org/licenses/by/4.0/>.

References

- Voigt, C., Kleine, J., Sauer, D., Moore, R.H., Bräuer, T., Le Clercq, P., Kaufmann, S., Scheibe, M., Jurkat-Witschas, T., Aigner, M., Bauder, U., Boose, Y., Borrmann, S., Crosbie, E., Diskin, G.S., DiGangi, J., Hahn, V., Heckl, C., Huber, F., Nowak, J.B., Rapp, M., Rauch, B., Robinson, C., Schripp, T., Shook, M., Winstead, E., Ziemba, L., Schlager, H., Anderson, B.E.: Cleaner burning aviation fuels can reduce contrail cloudiness. *Commun Earth Environ.* (2021). <https://doi.org/10.1038/s43247-021-00174-y>
- Bock, L., Burkhardt, U.: Contrail cirrus radiative forcing for future air traffic. *Atmos. Chem. Phys.* **19**, 8163–8174 (2019). <https://doi.org/10.5194/acp-19-8163-2019>
- Bührke T. and Meyer M.: Klimawirkungen des Luftverkehrs. Buch- und Offsetdruckerei Richard Thierbach GmbH, Köln. (2007).
- Kärcher, B., Yu, F.: Role of aircraft soot emissions in contrail formation. *Geophys. Res. Lett.* (2009). <https://doi.org/10.1029/2008GL036649>
- Kärcher, B.: Formation and radiative forcing of contrail cirrus. *Nat commun.* (2018). <https://doi.org/10.1038/s41467-018-04068-0>
- Marquart S.: Klimawirkung von Kondensstreifen: Untersuchungen mit einem globalen atmosphärischen Zirkulationsmodell. Dissertation, Ludwig-Maximilians-Universität, München. (2003).
- Appelman, H.: The formation of exhaust condensation trails by jet aircraft. *Am Meteorol Soc.* **34**(1), 14–20 (1953)
- Schuhmann, U.: On conditions for contrail formation from aircraft exhausts. *Meteorologische Zeitschrift* **5**, 4–23 (1996)
- Joos, F.: Technische verbrennung: verbrennungstechnik, verbrennungsmodellierung, emissionen. Springer, Berlin and Heidelberg (2006). (ISBN: 3540343334)
- Mishra, R.K., Chandel, S.: Soot formation and its effect in an aero gas turbine combustor. *Int J Turbo Jet-Eng* **36**(1), 61–73 (2019). <https://doi.org/10.1515/tjj-2016-0062>
- Warnatz, J., Maas, U., Dibble, R.W.: *Verbrennung: physikalisch-chemische Grundlagen, Modellierung und Simulation, Experimente, Schadstoff-Entstehung*, 3rd edn. Springer Verlag, Berlin, Heidelberg (2001)
- Tan, Y.R., Salamanca, M., Akroyd, J., Kraft, M.: How do the oxygenated functional groups in ether, carbonate and alcohol affect soot formation in Jet A2 diffusion flames? *Combust. Flame* (2022). <https://doi.org/10.1016/j.combustflame.2021.111849>
- Svensson, K.I., Richards, M., Mackrory, A., Tree, D.: Fuel composition and molecular structure effects on soot formation in direct-injection flames under diesel engine conditions. *SAE Tech Paper.* (2005). <https://doi.org/10.4271/2005-01-0381>
- Pélerin, D., Gaukel, K., Härtl, M., Jacob, E., Wachtmeister, G.: Potentials to simplify the engine system using the alternative diesel fuels oxymethylene ether OME1 and OME3–6 on a heavy-duty engine. *Fuel* **259**, 116231 (2020). <https://doi.org/10.1016/j.fuel.2019.116231>
- Andoga, R., Főző, L., Schrötter, M., Szabo, S.: The use of ethanol as an alternative fuel for small turbojet engines. *Sustainability* **13**(5), 2541 (2021). <https://doi.org/10.3390/su13052541>
- Kadlec, P., Henke, S., Bubník, Z.: Properties of ethanol and ethanol-water solutions—tables and equations. *Sugar Ind.* (2010). <https://doi.org/10.36961/si10420>
- Koegl, M., Mull, C., Baderschneider, K., Wislicenus, J., Will, S., Zigan, L.: Characterization of Nile red as a tracer for laser-induced fluorescence spectroscopy of gasoline and kerosene and their mixture with biofuels. *Sensors (Basel, Switzerland)* (2019). <https://doi.org/10.3390/s19122822>
- Härtl, M., Gaukel, K., Pélerin, D., Wachtmeister, G.: Oxymethylenether als potenziell CO₂-neutraler Kraftstoff für saubere Dieselmotoren Teil 1: Motoren-untersuchungen. *Motortech Z* **78**(2), 52–59 (2017). <https://doi.org/10.1007/s35146-016-0170-9>
- Oestreich D.: Prozessentwicklung zur Gewinnung von Oxymethylenethern (OME) aus Methanol und Formaldehyd. Dissertation, Karlsruher Institut für Technologie, Karlsruhe. (2017).
- Albrecht U., Schmidt P., Weindorf W., Wurster R., and Zittel W.: Kraftstoffstudie: Zukünftige Kraftstoffe für Verbrennungsmotoren und Gasturbinen—Abschlussbericht. (2013).
- Chevron. Aviation Fuels: Technical Review. San Ramon, Kalifornien. (2007).
- Bräunling, W.J.G.: *Flugzeug-triebwerke*. Springer, Berlin Heidelberg (2015). <https://doi.org/10.1007/978-3-642-34539-5>. (ISBN: 978-3-642-34538-8)
- Carvajal-Mariscal I., Sanchez Silva F., Jaramillo-Martínez R., and Polupan G.: Evaluation of ethanol as a fuel for gas turbines. In Proceedings of the ASME Power Conference—2013, New York, NY. (2014). ASME. Doi: <https://doi.org/10.1115/POWER2013-98162>.
- Chen, L., Zhang, Z., Lu, Y., Zhang, C., Zhang, X., Zhang, C., Roskilly, A.P.: Experimental study of the gaseous and particulate matter emissions from a gas turbine combustor burning butyl butyrate and ethanol blends. *Appl. Energy* **195**, 693–701 (2017). <https://doi.org/10.1016/j.apenergy.2017.03.075>
- Patra, J., Ghose, P., Datta, A., Das, M., Ganguly, R., Sen, S., Chatterjee, S.: Studies of combustion characteristics of kerosene ethanol blends in an axi-symmetric combustor. *Fuel* **144**, 205–213 (2015). <https://doi.org/10.1016/j.fuel.2014.12.036>

26. Pullman J.B.: Methanol, ethanol and jet fuel emissions comparison from a small gas turbine. In SAE Technical Paper Series, SAE Technical Paper Series. SAE International 400 Commonwealth Drive, Warrendale, PA, United States. DOI: <https://doi.org/10.4271/781013>. (1978)
27. Westerdahl, D., Fruin, S.A., Fine, P.L., Sioutas, C.: The Los Angeles International Airport as a source of ultrafine particles and other pollutants to nearby communities. *Atmos. Environ.* **42**(13), 3143–3155 (2008). <https://doi.org/10.1016/j.atmosenv.2007.09.006>
28. Karataş, A.E., Gülder, Ö.L.: Soot formation in high pressure laminar diffusion flames. *Prog. Energy Combust. Sci.* **38**(6), 818–845 (2012). <https://doi.org/10.1016/j.pecs.2012.04.003>
29. Condensation Particle Counter Model 3772/3771: Operation and Service Manual. TSI, Shoreview, MN, USA, 2015. Accessed: Aug. 11, 2023 [Online]. Available: https://www.kenelec.com.au/wp-content/uploads/2016/06/TSI_3771_3772_Manual.pdf.
30. Kinsey, J.S., Corporan, E., Pavlovic, J., DeWitt, M., Klingshirn, C., Logan, R.: Comparison of measurement methods for the characterization of the black carbon emissions from a t63 turboshaft engine burning conventional and fischer–tropsch fuels. *J. Air Waste Manag. Assoc.* **69**(5), 576–591 (2019). <https://doi.org/10.1080/10962247.2018.1556188>
31. Ogawa, H., Miyamoto, N., Yagi, M.: Chemical-kinetic analysis on PAH formation mechanisms of oxygenated fuels. SAE Tech Paper. (2003). <https://doi.org/10.4271/2003-01-3190>
32. Tan, Y.R., Salamanca, M., Akroyd, J., Kraft, M.: Supplementary Material to How do the oxygenated functional groups in ether, carbonate and alcohol affect soot formation in Jet A2 diffusion flames? *Combust. Flame* (2022). <https://doi.org/10.1016/j.combustflame.2021.111849>
33. Tan, Y.R., Botero, M., Sheng, Y., Dreyer, J., Xu, R., Yang, W.M., Kraft, M.: Sooting characteristics of polyoxymethylene dimethyl ether blends with diesel in a diffusion flame. *Fuel* **224**, 499–506 (2018). <https://doi.org/10.1016/j.fuel.2018.03.051>

Publisher's Note Springer Nature remains neutral with regard to jurisdictional claims in published maps and institutional affiliations.